Journal of Power Sources 196 (2011) 4905–4910

Contents lists available at ScienceDirect

Journal of Power Sources

journal homepage: www.elsevier.com/locate/jpowsour

# A comparative study of Pt/C cathodes in $Sn_{0.9}In_{0.1}P_2O_7$ and $H_3PO_4$ ionomers for high-temperature proton exchange membrane fuel cells

Y.C. Jin, M. Okada, T. Hibino*

*Graduate School of Environmental Studies, Nagoya University, Nagoya, Aichi 464-8601, Japan*

ARTICLE INFO

*Article history:*
Received 20 December 2010
Received in revised form 24 January 2011
Accepted 7 February 2011
Available online 16 February 2011

*Keywords:*
Cathode
High-temperature operation
$Sn_{0.9}In_{0.1}P_2O_7$
Sulfonated polystyrene-b-poly(ethylene/butylene)-b-polystyrene

ABSTRACT

New Pt/C cathodes with many reaction sites for the oxygen reduction reaction as well as high tolerance to Pt corrosion have been designed for high-temperature proton exchange membrane fuel cells (PEMFCs), wherein a composite mixture of $Sn_{0.9}In_{0.1}P_2O_7$ (SIPO) and sulfonated polystyrene-b-poly(ethylene/butylene)-b-polystyrene (sSEBS) functioned as an ionomer. The microstructure of the Pt-SIPO-sSEBS/C cathode was characterized by homogeneous distribution of the ionomer over the catalyst layer and close contact between the ionomer and the Pt/C powder. As a result, the activation and concentration overpotentials of the Pt-SIPO-sSEBS/C cathode between 100 and 200 °C were lower than those of an $H_3PO_4$-impregnated Pt/C cathode, which suggests that the present ionomer can avoid poisoning of Pt by phosphate anions and the limitation of gas diffusion through the catalyst layer. Moreover, agglomeration of Pt in the Pt-SIPO-sSEBS/C cathode was not observed during a durability test at 150 °C for 6 days, although it was significant in the Pt-$H_3PO_4$/C cathode. Therefore, it is concluded that the Pt-SIPO-sSEBS/C electrode is a very promising cathode candidate for high-temperature PEMFCs.



## 1. Introduction

In recent years, there has been significant interest in the development of high-temperature (>100 °C) proton exchange membrane fuel cells (PEMFCs) [1,2]. Operating a fuel cell at elevated temperatures provides the anode catalyst with high tolerance to CO, eliminating the need for a CO-removal unit. In addition, the electrode reaction kinetics are enhanced, permitting low Pt loading. Other advantages include simplified water management, good drainage at the cathode, and effective heat dissipation. Among such PEMFC systems, solid acid fuel cells have been intensively investigated over the past decade. Various types of solid acids have been reported to exhibit relatively high proton conductivity ($10^{-3}$–$10^{-1}$ S cm$^{-1}$) at low humidities [3–11]. More recently, thin solid acid membranes have also been fabricated by compositing solid acid powers with organic binders or substrates [12–14].

In spite of these efforts, the power output and durability of solid acid fuel cells remain strongly dependent on the catalytic activity and thermo-chemical stability, respectively, of the cathode used [15]. The cathode commonly comprises Pt, carbon, and a proton-conductive ionomer. Liquid $H_3PO_4$ [16,17] and electrolyte components [18–20] are usually employed as ionomers in solid acid fuel cells. Although the $H_3PO_4$ ionomer can be homogeneously distributed over the catalyst layer, providing a number of reaction sites for the oxygen reduction reaction (ORR), it faces a serious challenge in that the Pt particle is easily corroded [21]. Other challenges for the $H_3PO_4$ ionomer include poisoning of the Pt catalyst by strong adsorption of phosphate anions [22] and low oxygen solubility in $H_3PO_4$ [23]. In contrast, because the solid acid ionomers are tightly fixed in the catalyst layer, they are not washed away from the cathode. However, it is difficult to form continuous three-dimensional networks of the solid acid ionomer through the pores of the catalyst layer, due to which proton transfer is interrupted [18,19]. Accordingly, the chemical, structural, and thermal properties of the ionomer used are very important factors for determining the cathode performance and lifetime.

From the above discussion, it is clear that a better ionomer needs to be developed for practical applications of solid acid fuel cells. In this study, we attempted to design a new ionomer that overcomes the disadvantages of $H_3PO_4$ and solid acid ionomers while incorporating their advantages. Our approach is to use an elastic composite ionomer comprising a solid acid and an organic binder. This offers the possibility that this ionomer can spread widely within a catalyst layer, such as $H_3PO_4$, and attach tightly to the Pt/C powder, such as solid acids. The solid acid used in this study was $Sn_{0.9}In_{0.1}P_2O_7$ (SIPO) powder that shows high proton conductivities (~0.1 S cm$^{-1}$) between 100 and 300 °C in dry and wet conditions [10]. A unique feature of this material is that the conductivity increases monotonically with increasing temperature [24], which is different from superprotonic behavior that shows a sharp increase in the conductivity of some orders of magnitude by structural transition from a low- to a high-temperature phase [3,9]. Three candidate

* Corresponding author. Tel.: +81 52 789 4888; fax: +81 52 789 4894.
*E-mail address:* hibino@urban.env.nagoya-u.ac.jp (T. Hibino).

0378-7753/$ – see front matter © 2011 Elsevier B.V. All rights reserved.
doi:10.1016/j.jpowsour.2011.02.028

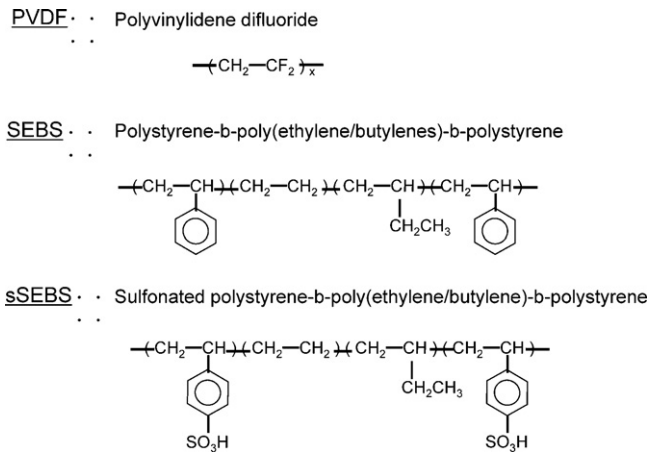


**Fig. 1.** Chemical structures of PVDF, SEBS, and sSEBS.

binders were investigated to search for a composite ionomer with good mechanical stability, including polyvinylidene difluoride (PVDF), polystyrene-b-poly(ethylene/butylenes)-b-polystyrene (SEBS), and sulfonated polystyrene-b-poly(ethylene/butylene)-b-polystyrene (sSEBS), shown in Fig. 1. $H_3PO_4$ was also tested as an ionomer for comparison with the obtained composite ionomers for catalytic properties and deterioration of the cathode.

## 2. Experimental

### 2.1. Preparation of cathodes

The cathodes were synthesized as follows. SIPO was obtained in the same manner as reported previously [10]. 4.0 g of SIPO powder was ground in 20.0 g of tetrahydrofuran (THF) using a planetary ball mill at 150 rpm for 16 h. THF was also used as a solvent for dissolving PVDF (Gunze Limited), SEPS, or sSEBS (Kuraray Co. Ltd.). Binder (1.0 g each) was added to 20.0 g of THF while stirring at room temperature until a homogeneous solution was formed. Pt/C powder (0.067 g; 30 wt% Pt, Tanaka Kikinzoku Kogyo) was also suspended in 4.480 g of THF. Catalyst inks with different weight ratios (Pt/C:SIPO:binder = 2:(1 − $x$):$x$) were prepared by mixing appropriate quantities of SIPO slurry, binder solution and Pt/C suspension in THF using an ultrasonic bath for 20 min. Each ink was then painted on the surface of a gas diffusion layer (Toray TGPH-090) using a spray coating technique, followed by heating at 50 °C in atmospheric air for 10 min. The Pt loading was adjusted to be around 0.6 mg cm$^{-2}$ by controlling the spray time. For comparison, a commercially available Pt/C (BASF, Pt loading: 0.6 mg cm$^{-2}$) was impregnated with supersaturated 105% $H_3PO_4$ at 130 °C overnight.

### 2.2. Characterizations of cathodes

The microstructures of the as-prepared cathodes were analyzed using X-ray diffraction (XRD) and scanning electron microscopy (SEM). The XRD patterns were recorded using a Rigaku Miniflex II instrument with Cu Kα radiation (λ = 1.5432 Å) as the X-ray source. The diffractometer was operated at 45 kV and 20 mA. SEM images were obtained using a Hitachi S-4800 microscope at an accelerating voltage of 15 kV with a beam current of 0.2 nA. The agglomeration of Pt particles in the cathodes was also measured as follows. The cathodes were kept on the surface of a pressed electrolyte, which will be described later, in air at 150 °C for 6 days. Subsequently, the size of the Pt particle was determined from the half-value width of the (1 1 1) XRD peak, and the distribution of the Pt particles was observed using transmission electron microscopy (TEM). Bright-field transmission images were obtained using a Jeol JEM2100F microscope at an accelerating voltage of 200 kV with a beam current of 92 μA.

### 2.3. Electrochemical measurements

A pressed SIPO pellet (thickness: ~1 mm) and a SIPO-polystyrene-b-poly(ethylene/propylene)-b-polystyrene (SEPS) composite membrane (80 wt% SIPO, thickness: ~60 μm) were used as electrolytes for the cathode polarization measurements and fuel cell tests, respectively. The preparation methods of these electrolytes have been described in our previous studies [10,14]. For both measurements, an ionomer-free Pt/C anode (Pt loading: 0.6 mg cm$^{-2}$) obtained from BASF was used. The cathodic overpotential was measured using the following procedure. The anode and cathode (area: 0.5 cm$^2$) were arranged on opposite sides of the pressed electrolyte. Two gas chambers were set up by placing the cell assembly between two alumina tubes. The anode and cathode chambers were supplied with non-humidified hydrogen and air, respectively, at a flow rate of 30 mL min$^{-1}$ in the temperature range 100–200 °C. The overpotentials of the cathodes were analyzed using the current interruption method, wherein a sharp change in voltage corresponds to ohmic loss, and a slow voltage change corresponds to non-ohmic polarization losses (activation and concentration). In the present case, an Au reference electrode was attached to the surface on the side of the electrolyte. The exchange current density, $i_0$, for the cathode was estimated using the following equation [25]:

$$\eta = -\frac{RT}{\alpha nF \ln(i_0)} + \frac{RT}{\alpha nF \ln(i)} \quad (1)$$

where $\eta$ is the overpotential, $R$ is the gas constant, $F$ is the Faraday constant, $n$ is the number of exchanged electrons, $\alpha$ is the transfer coefficient, and $i$ is the current density. Fuel cell tests were carried out using the four-probe method. The electrolyte membrane was sandwiched between the two electrodes (area: 0.5 cm$^2$) and hot-pressed at 120 °C at 0.8 MPa for 30 s. A hydrogen/air fuel cell was set up in the same manner as above. The discharge properties of the fuel cell were measured at temperatures from 100 to 200 °C using a Hokuto Denko HA-501 galvanostat. The durability of the fuel cell was also measured by monitoring the cell voltage while maintaining a constant current density at 150 °C for 50 h. The impedance spectra before and after the durability tests were acquired using a Solartron SI 1260 impedance/gain-phase analyzer with an AC amplitude of 20 mV at frequencies ranging from 100 kHz to 0.1 Hz.

## 3. Results and discussion

### 3.1. Polarization properties of cathodes

The ORR activity of the Pt-SIPO-PVDF, -SEBS, and -sSEBS/C cathodes with a weight ratio of Pt/C:SIPO:binder = 2:0.5:0.5 at a temperature of 150 °C is shown in Fig. 2(a), in addition to the data for the Pt-$H_3PO_4$/C and ionomer-free Pt/C cathodes. The overpotential and current relationships were not linear, especially at low currents, for all the cathodes tested, which indicates that the activation overpotential was dominant. The overpotential decreased in the order Pt-SIPO-PVDF/C > Pt/C > Pt-SIPO-SEBS/C > Pt-$H_3PO_4$/C > Pt-SIPO-sSEBS/C. This same order was observed at 100 and 200 °C, although we could not exactly measure the overpotential of the Pt-SIPO-PVDF/C at 100 °C because of its very unstable behavior. It is worth noting that the Pt-SIPO-sSEBS/C cathode exhibited a higher ORR activity than the Pt-$H_3PO_4$ cathode. This will be further discussed later. To clarify how each ionomer contributes to the enhancement of ORR activity, $i_0$ was estimated for the five

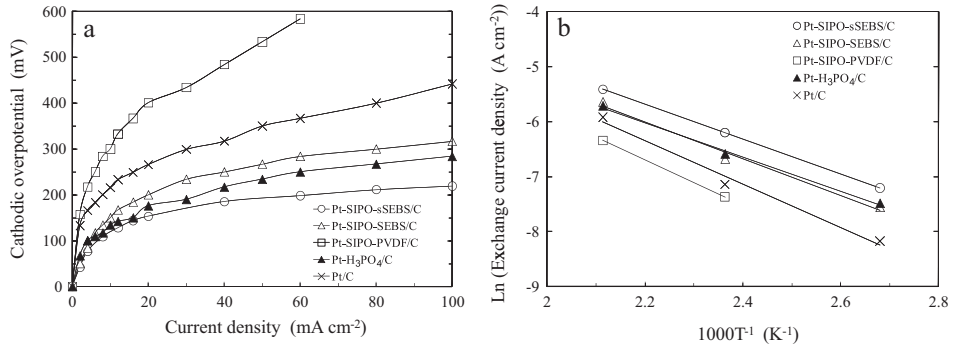


**Fig. 2.** (a) Cathodic overpotentials at 150 °C and (b) Arrhenius plots of the exchange current density for Pt-SIPO-sSEBS/C, Pt-SIPO-SEBS/C, Pt-SIPO-PVDF/C, Pt-$H_3PO_4$/C, and Pt/C.

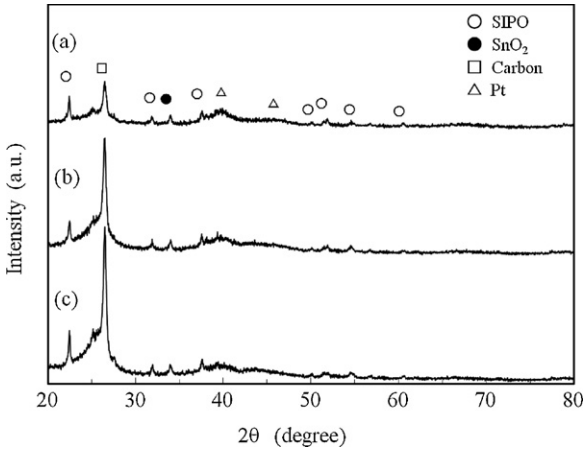


**Fig. 3.** XRD patterns of (a) Pt-SIPO-sSEBS/C, (b) Pt-SIPO-SEBS/C, and (c) Pt-SIPO-PVDF/C.

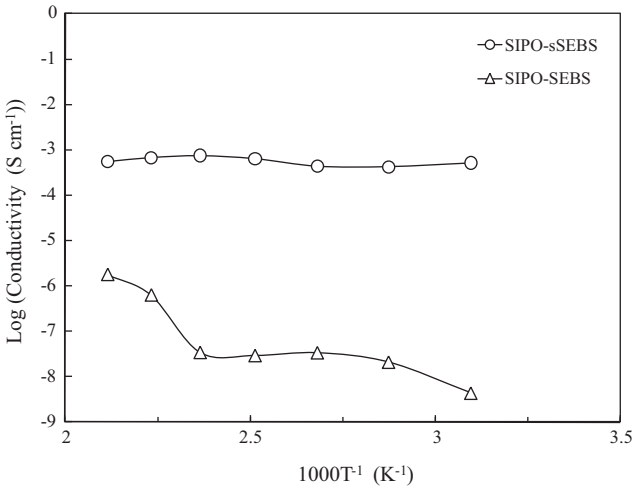


**Fig. 5.** Arrhenius plots of proton conductivity for SIPO-sSEBS and -SEBS composite ionomers.

cathodes. As seen in Fig. 2(b), the activation energies obtained from the slopes of the Arrhenius plots were similar for each cathode (~30 kJ $mol^{-1}$), which suggests that the same reaction mechanism for the ORR was operating at the five cathodes. We speculate that the differences in the $i_0$ values among the five cathodes arise from differences in the frequency factor, *A*. The *A* value may also be considered to reflect the number of reaction sites at the cathode. On the other hand, the $i_0$ value and the Tafel slop obtained for the Pt-SIPO-sSEBS/C cathode at 200 °C were 4.47 mA $cm^{-2}$ and 145 mV $decade^{-1}$, respectively. These properties are more favorable as a cathode than the corresponding data reported for an ionomer-free Pt/C cathode at 200 °C [26], which confirms the validity of our measurements.

### 3.2. Characterizations of cathodes

The Pt-SIPO-PVDF, -SEBS, and -sSEBS/C cathodes with the same weight ratio as above were characterized using XRD and SEM. Fig. 3 indicates that all of the diffraction peaks observed for the three cathodes could be assigned to either SIPO, $SnO_2$, carbon, or Pt. ($SnO_2$ still remains in the bulk of the SIPO particles because of the formation of a core–shell structure [27].) The peak intensities of these components, except for carbon, were comparable among the three cathode samples. In contrast, Fig. 4 reveals a large difference in the surface morphology for the three cathodes. Whereas the Pt-SIPO-SEBS and -sSEBS/C cathodes showed high porosity with pore dimensions of several micrometers or larger, the Pt-SIPO-PVDF/C cathode was visually observed to be non-porous and significantly cracked. It appears that in the case of the Pt-SIPO-PVDF/C cathode, gas diffusivity and permeability are very poor, thereby resulting in the extremely low ORR activity observed (Fig. 2). In other words, it is suggested that the difference in ORR activity between the Pt-SIPO-SEBS and -sSEBS (Fig. 2) is not primarily due to the difference in their microstructure and morphology.

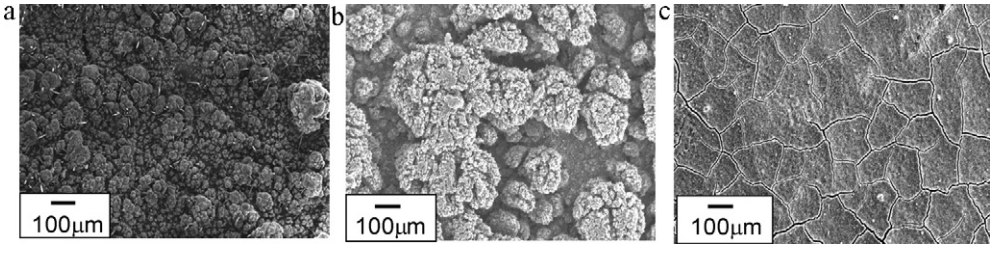


**Fig. 4.** SEM images of (a) Pt-SIPO-sSEBS/C, (b) Pt-SIPO-SEBS/C, and (c) Pt-SIPO-PVDF/C.

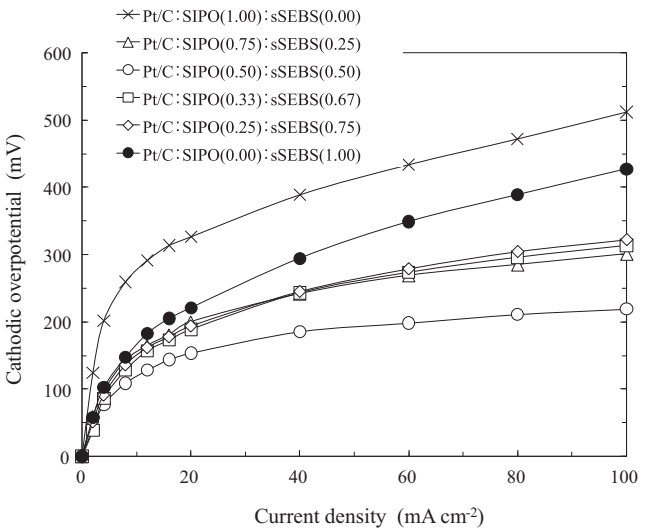


**Fig. 6.** Cathodic overpotentials of Pt-SIPO-sSEBS/C with various weight ratios.

Unlike SEBS, sSEBS has acidic functions as proton sites (Fig. 1). There is the possibility that such acidic functions permit additional proton transfer in the Pt-SIPO-sSEBS/C cathode. To confirm this possibility, the proton conductivity of the SIPO-sSEBS ionomer with a weight ratio SIPO:sSEBS = 0.5:0.5 was compared with that of the SIPO-SEBS ionomer with the same weight ratio as above in non-humidified air. Fig. 5 shows that the proton conductivities of the SIPO-sSEBS ionomer were several orders of magnitude higher than those of the SIPO-SEBS ionomer over a wide temperature range (50–200 °C). It is probable that the acidic functions form a proton-conducting pathway from one SIPO cluster to another. It is thus concluded that the good performance of the Pt-SIPO-sSEBS/C cathode is attributable to its relatively high proton conductivity. Subsequent experiments were therefore performed using the Pt-SIPO-sSEBS/C cathode.

### 3.3. Optimization of cathode

The Pt-SIPO-sSEBS/C cathodes with various weight ratios (Pt/C:SIPO:sSEBS = 2:(1 − *x*):*x*) were investigated to optimize the SIPO and sSEBS contents. The overpotentials of the Pt-SIPO-sSEBS/C cathodes at a temperature of 150 °C are shown in Fig. 6. The overpotential decreased with increasing *x* value, reached a minimum at *x* = 0.5, and subsequently increased. Accordingly, the optimal weight ratio of SIPO:sSEBS was determined to be 0.5:0.5. It should be noted that the overpotentials of the Pt-SIPO/C (*x* = 0) and Pt-sSEBS/C (*x* = 1) were much larger than those of all the Pt-SIPO-sSEBS/C cathodes. These behaviors can be explained by the cross-sectional SEM images of the Pt-SIPO-sSEBS/C (*x* = 0.5), Pt-SIPO/C, and Pt-sSEBS/C cathodes, shown in Fig. 7. By comparing the microstructures of the Pt-SIPO-sSEBS/C and Pt-SIPO/C cathodes, it is seen that while approximately 400-nm-sized SIPO particles were clearly visualized in the Pt-SIPO/C matrix (Fig. 7(b)), the SIPO particles were almost perfectly covered with both the Pt/C powders and the sSEBS binders in the Pt-SIPO-sSEBS/C (Fig. 7(c)). More importantly, the aggregates comprised of the three components were more closely connected to each other in the Pt-SIPO-sSEBS/C matrix, compared with the SIPO particles in the Pt-SIPO/C matrix. It is suggested that the number of reaction sites for ORR is much larger for the Pt-SIPO-sSEBS/C than for the Pt-SIPO/C. On the other hand, the Pt/C powders were packed with the sSEBS binder in the Pt-sSEBS/C matrix (Fig. 7(a)), wherein the supply of oxygen molecules to the reaction sites was likely insufficient. In addition, because the proton conductivity of sSEBS at 150 °C is as low as $\sim 10^{-5}$ S cm$^{-1}$ [28], sSEBS alone cannot function as the ionomer. These results demonstrate that the combination of SIPO and sSEBS is necessary to develop a promising ionomer for solid acid fuel cells.

### 3.4. Performance of cathode

To better understand the cathode performance, a hydrogen/air fuel cell was fabricated with the Pt-SIPO-sSEBS cathode, and the discharge properties were measured at temperatures in the range from 100 to 200 °C. The cell voltage and power density versus the current density are shown in Fig. 8, including the data for the fuel

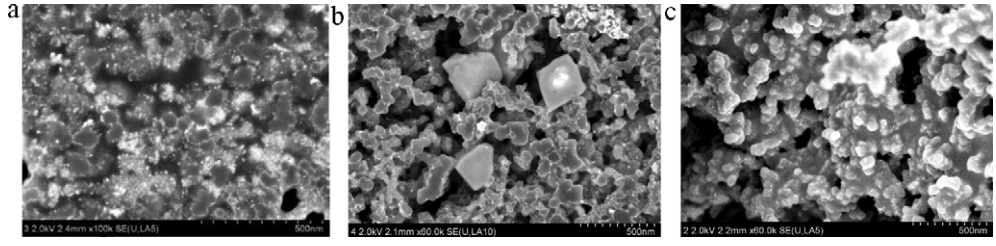


**Fig. 7.** Cross-sectional SEM images of (a) Pt-sSEBS/C, (b) Pt-SIPO/C, and (c) Pt-SIPO-sSEBS/C.

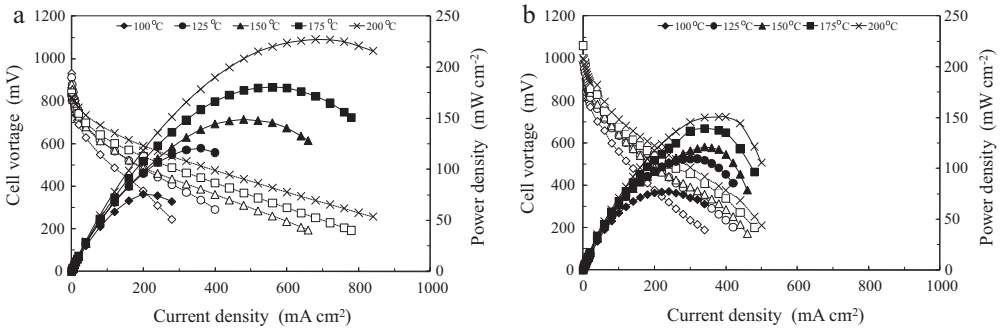


**Fig. 8.** Cell voltages and power densities versus current density of hydrogen/air fuel cells with the (a) Pt-SIPO-sSEBS/C and (b) Pt-$H_3PO_4$/C cathodes.

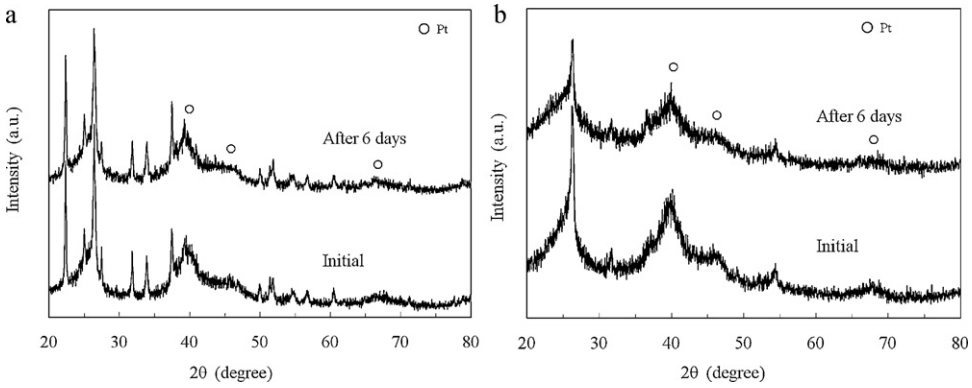


**Fig. 9.** XRD patterns of (b) Pt-SIPO-sSEBS/C and (b) Pt-$H_3PO_4$/C before and after exposure to air at 150 °C for 6 days.

cell with the Pt-$H_3PO_4$/C cathode. As expected, the fuel cell with the Pt-SIPO-sSEBS/C cathode exhibited higher power densities, compared to the fuel cell with the Pt-$H_3PO_4$/C cathode. This clearly reflects the difference in cathodic overpotential between the two electrodes, which is significant especially at low and high current densities. We can associate the large overpotential observed for the Pt-$H_3PO_4$/C cathode at low current densities with a high energy barrier of the charge-transfer reaction, which probably results from poisoning of the Pt catalyst due to strong adsorption of phosphate anions [22]. We can also relate the large overpotential observed for the Pt-$H_3PO_4$/C cathode at high current densities to high gas transport resistance through the electrodes, which is likely due to the low oxygen solubility in $H_3PO_4$ [23]. It is thus concluded that the use of the SIPO-sSEBS ionomer could successfully overcome these disadvantages. However, the open-circuit voltages (OCVs) of the fuel cell with the Pt-SIPO-sSEBS/C cathode were somewhat lower than those of the fuel cell with the Pt-$H_3PO_4$/C cathode. One reason for this is that a part of $H_3PO_4$ in the Pt-$H_3PO_4$/C cathode penetrates into the cathode side of the electrolyte membrane, which prevents physical leakage of gas through the electrolyte membrane. Indeed, the fuel cell with an ionomer-free Pt/C cathode also showed comparable OCVs at all the temperatures tested, compared to the fuel cell with the Pt-SIPO-sSEBS/C cathode.

### 3.5. Stability of cathode

Finally, the stability of the Pt-SIPO-sSEBS/C cathode was investigated under two operating conditions, open-circuit and discharge. After keeping the Pt-SIPO-sSEBS/C and Pt-$H_3PO_4$/C cathodes under open-circuit conditions at 150 °C, the agglomeration of Pt particles

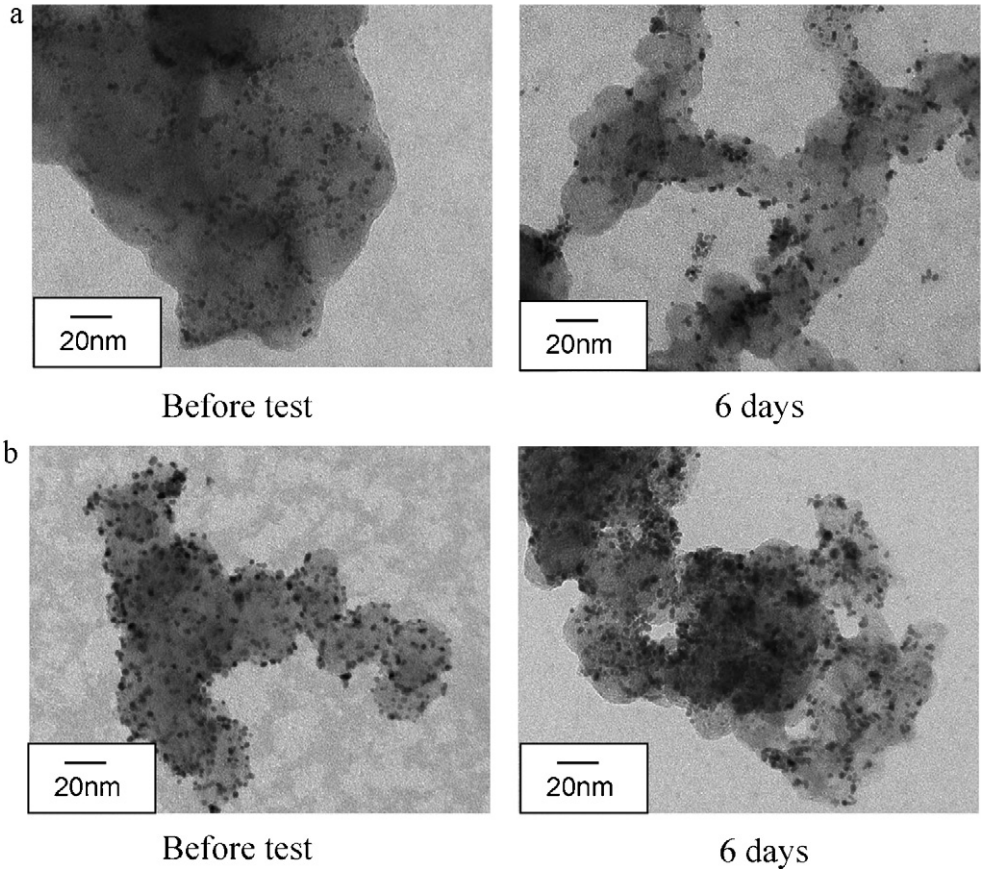


**Fig. 10.** TEM images of (b) Pt-SIPO-sSEBS/C and (b) Pt-$H_3PO_4$/C before and after exposure to air at 150 °C for 6 days.

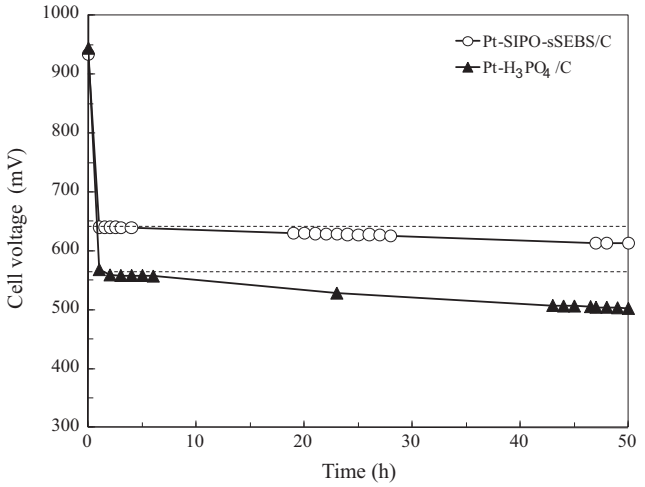


**Fig. 11.** Changes in the cell voltages of hydrogen/air fuel cells with Pt-SIPO-sSEBS/C and Pt-$H_3PO_4$/C cathodes at 150 °C. The current density was kept at a constant value of 100 mA $cm^{-2}$.

in each cathode was analyzed using XRD measurements. It can be seen from Fig. 9 that the XRD patterns of Pt in the Pt-SIPO-sSEBS/C cathode showed no significant change after the measurements, whereas the diffraction peaks of Pt were considerably decreased for the Pt-$H_3PO_4$/C cathode after 6 days. The average particle size of Pt in all the cathodes were estimated from the Scherrer formula to be 4.20 and 4.26 nm for the Pt-SIPO-ssEBS/C before and after the measurements, respectively, and 4.57 and 7.59 nm for the Pt-$H_3PO_4$/C before and after the measurements, respectively. These samples were also characterized using TEM, and the results are shown in Fig. 10. By comparing the TEM images of the Pt-SIPO-sSEBS/C and Pt-$H_3PO_4$/C cathodes after the measurements, it is obvious that agglomeration of Pt particles was more significant in the Pt-$H_3PO_4$/C cathode than in the Pt-SIPO-sSEBS/C cathode. A similar result for the Pt-$H_3PO_4$/C cathode in air at elevated temperatures was reported by Honji et al. [21]. According to the mechanism proposed by them, the agglomeration of Pt particles occurs via dissolution of Pt into $H_3PO_4$ and subsequent redeposition of the dissolved Pt, which is also applicable in the present case. This suggests that the high stability of the Pt-SIPO-sSEBS/C cathode in air at elevated temperatures can be attributed to the low solubility of Pt in the SIPO-sSEBS ionomer or the low acidity of this ionomer.

The cell voltage of the fuel cells with the Pt-SIPO-sSEBS/C and Pt-$H_3PO_4$ cathodes was monitored during cell discharge at 150 °C. In Fig. 11, the stability of the cell voltage was found be almost independent of the cathode used. The cell voltages with the Pt-SIPO-sSEBS and Pt-$H_3PO_4$ cathodes gradually decreased, although the decrement was somewhat less for the Pt-SIPO-sSEBS/Pt cathode than for the Pt-$H_3PO_4$/C cathode. Impedance measurements showed that the decrease in cell voltage was mainly attributable to an increase in the polarization resistance rather than the ohmic resistance; for example, the polarization resistance of the Pt-SIPO-sSEBS/C cathode increased from 1.5 to 2.1 Ω $cm^2$. Because the dissolution of Pt in acid solutions is considerable when the cathode potential is over 800 mV [21], it is reasonable to consider that the deterioration observed above is not mainly due to the agglomeration of the Pt particles during cell discharge. One possible explanation is that a part of the amorphous carbon in the catalyst support is transformed into graphitic carbon, resulting in a significant decrease in the surface area of carbon [29]. If this is true, then one could avoid such deterioration by using a graphite-rich catalyst support. Therefore, further research is required in catalyst development to improve the stability of the cathode during cell discharge in these fuel cells.

## 4. Conclusions

A composite cathode was successfully fabricated using SIPO powder and sSEBS as the binder. The use of this ionomer enhanced both the porosity of the cathode and proton conductivity in the cathode. Moreover, homogeneously connected networks of proton pathways were obtained in the cathode. The resultant ORR activity of the Pt-SIPO-sSEBS/C cathode was higher than that of the Pt-$H_3PO_4$/C cathode between 100 and 200 °C, thereby yielding better discharge properties under high-temperature PEMFC conditions. In particular, it is noteworthy that polarization losses at low and high current densities were significantly reduced by using the Pt-SIPO-sSEBS/C cathode. Another beneficial effect of this ionomer was less agglomeration of Pt particles compared to that in the $H_3PO_4$ ionomer. This characteristic was responsible for the low solubility of Pt in the SIPO-sSEBS ionomer or the low acidity of this ionomer.

## References

[1] Q. Li, R. He, J.O. Jensen, N.J. Bjerrum, Chem. Mater. 15 (2003) 4896–4915.
[2] J. Zhang, Z. Xie, J. Zhang, Y. Tang, C. Song, T. Navessin, Z. Shi, D. Song, H. Wang, D.P. Wilkinson, Z. Liu, S. Holdcroft, J. Power Sources 160 (2006) 872–891.
[3] S.M. Haile, D.A. Boysen, C.R.I. Chisholm, R.B. Merle, Nature 410 (2001) 910–913.
[4] W. Wieczorek, G. Zukowska, R. Borkowska, S.H. Chung, S. Greenbaum, Electrochim. Acta 46 (2001) 1427–1438.
[5] A. Matsuda, T. Kanzaki, K. Tadanaga, M. Tatsumisago, T. Minami, Solid State Ionics 154–155 (2002) 687–692.
[6] T. Matsui, S. Takeshita, Y. Iriyama, T. Abe, M. Inaba, Z. Ogumi, Electrochem. Commun. 6 (2004) 180–182.
[7] J.D. Kim, I. Honma, Electrochim. Acta 49 (2004) 3179–3183.
[8] C. Yang, S. Srinivasan, A.B. Bocarsly, S. Tulyani, J.B. Benziger, J. Membr. Sci. 237 (2004) 145–161.
[9] D.A. Boysen, T. Uda, C.R.I. Chisholm, S.M. Haile, Science 303 (2004) 68–70.
[10] M. Nagao, A. Takeuchi, P. Heo, T. Hibino, M. Sano, A. Tomita, Electrochem. Solid-State Lett. 9 (2006) A105–A109.
[11] Y. Aoki, H. Habazaki, T. Kunitake, J. Am. Chem. Soc. 131 (2009) 14399–14406.
[12] J.D. Kim, T. Mori, I. Honma, J. Electrochem. Soc. 153 (2006) A508–A514.
[13] M.Q. Li, K. Scott, Electrochem. Solid-State Lett. 12 (2009) B171–B175.
[14] Y.C. Jin, T. Hibino, Electrochim. Acta 55 (2010) 8371–8375.
[15] S.M. Haile, C.R.I. Chisolm, K.A. Sasaki, D.A. Boysen, T. Uda, Faraday Discuss. 134 (2007) 17–39.
[16] M.Q. Li, Z.G. Shao, K. Scott, J. Power Sources 183 (2008) 69–75.
[17] S.Y. Oh, T. Yoshida, G. Kawamura, H. Muto, M. Sakai, A. Matsuda, J. Mater. Chem. 20 (2010) 6359–6366.
[18] P. Heo, T. Harada, T. Hibino, Electrochem. Solid-State Lett. 12 (2009) B1–B4.
[19] T. Harada, Y.C. Jin, P. Heo, T. Hibino, Fuel Cells 10 (2010) 798–803.
[20] Á. Varga, N.A. Brunelli, M.W. Louie, K.P. Giapis, S.M. Haile, J. Mater. Chem. 20 (2010) 6309–6315.
[21] A. Honji, T. Mori, K. Tamura, Y. Hishinuma, J. Electrochem. Soc. 135 (1988) 355–359.
[22] P. Zelenay, B.R. Scharifker, J.O'M. Bockris, J. Electrochem. Soc. 133 (1986) 2262–2267.
[23] Z. Liu, J.S. Wainright, M.H. Litt, R.F. Savinell, Electrochim. Acta 51 (2006) 3914–3923.
[24] Y.C. Jin, Y.B. Shen, T. Hibino, J. Mater. Chem. 20 (2010) 6214–6217.
[25] S. Haji, Renewable Energy 36 (2011) 451–458.
[26] S. Yoshimi, T. Matsui, R. Kikuchi, K. Eguchi, J. Power Sources 179 (2008) 497–503.
[27] R. Lan, S. Tao, J. Alloys Compd. 486 (2009) 380–385.
[28] Y.C. Jin, K. Fujiwara, T. Hibino, Electrochem. Solid-State Lett. 13 (2010) B8–B10.
[29] G.A. Gruver, J. Electrochem. Soc. 125 (1978) 1719–1720.